Journal of Solid State Chemistry 184 (2011) 1008–1015

Contents lists available at ScienceDirect

Journal of Solid State Chemistry

journal homepage: www.elsevier.com/locate/jssc

Alginate hydrogel-mediated crystallization of calcium carbonate

Yufei Ma, Qingling Feng *

State Key Laboratory of New Ceramics and Fine Processing, Department of Materials Science and Engineering, Tsinghua University, Haidian District, Beijing 100084, PR China

ARTICLE INFO

Article history:
Received 2 September 2010
Received in revised form
31 January 2011
Accepted 3 March 2011
Available online 15 March 2011

Keywords:
Calcium carbonate
Alginate hydrogel
In vitro study
Biomineralization mechanism

ABSTRACT

We documented a specific method for combining calcium ions and alginate molecules slowly and continuously in the mineralization system for the purpose of understanding the mediating function of alginate on the crystallization of calcium carbonate. The alginate was involved in the nucleation and the growth process of $CaCO_3$. The crystal size, morphology and roughness of crystal surface were significantly influenced by the type of the alginate, which could be accounted for by the length of the G blocks in alginate. A combination of Fourier transform infrared spectroscopy and thermogravimetric analysis showed that there were the chemical interactions between the alginate and the mineral phase. This strategic approach revealed the biologically controlled $CaCO_3$ mineralization within calcium alginate hydrogels via the selective nucleation and the confined crystallization of $CaCO_3$. The results presented here could contribute to the understanding of the mineralization process in hydrogel systems.

1. Introduction

Biomineralization process is a specific process that applies natural macromolecule to control and direct the crystallization of biominerals. The formation of various biominerals in living organisms is based on the biomineralization process [1]. Hence, the ability to control crystallization is a critical requirement in the deposition of many important biominerals. Calcium carbonate is of great interest in the context of crystal control because it is produced by a wide variety of biological organisms that exhibit exquisite control over the polymorph, location of nucleation, crystal size and morphology [2].

Calcium carbonate is one of the most wide-spreading minerals, which can exist in several different polymorphs (in the order of increasing stability): vaterite, aragonite and calcite. Usually, these are found in polycrystalline spherulites, needle-like particles and single-crystalline cubes, respectively. In nature, however, the morphology is precisely controlled by organic molecules and the mineral is designed to meet the structural and functional needs of the organism [1]. Although aragonite and calcite are the most commonly-found polymorphs in natural systems, vaterite is also present in some organisms. All of the polymorphs can be obtained within *in vitro* crystallization. All of the polymorphs eventually transform into the most stable form, calcite, in the presence of water.

The precise control of additives has inspired many researchers to investigate the influence of additives on the crystallization/growth of calcium carbonate [3–10]. A number of additives, such as synthetic polymers [6,9–13] and biopolymers [14–17], have been proven to exert effects on the polymorphs and morphologies of $CaCO_3$. Most of the studies are concentrated on the role of proteins. Polysaccharide, as a kind of natural biopolymer, has also been shown to play a vital role in the growth of biominerals in organisms [18]. In recent publications natural chitin has been used, as a representative of polysaccharide, for the controlled deposition of calcium carbonate [19–23]. Falini et al. [19] observed three main polymorphs of calcium carbonate crystals, such as calcite, aragonite and vaterite, in the β-chitin scaffold. Their location within the matrix is a function of the polymorph. The supersaturation inside the compartmentalized space in the chitin governs the location and polymorphism of the crystals. Yamamoto et al. [20] previously reported that the nucleation of $CaCO_3$ occurred in the liquid-crystalline chitin matrix and the $CaCO_3$ crystals deposited in the chitin gels to form hybrids with an interpenetrated three-dimensional structure. However, little is known about the precise mechanism on how polysaccharides affect the crystallization of $CaCO_3$. From the viewpoint of chemical structure, many polysaccharides are natural block copolymers and consist of two or more different glycosidic monomer units [2]. For example, alginate is a hydrophilic polysaccharide that is produced by algae and bacteria. Chemically, it is a linear copolymer of two monomers, α-L-guluronic acid (G) and β-D-mannuronic acid (M) residues, joined by glycosidic links α-1, 4 and β-1, 4. The monomers are arranged in a block-wise pattern along the chain with homopolymeric regions of G and M, termed G and M blocks, respectively, interspaced with regions of alternating structure (GM blocks) [24]. The ratio and order of G and M units

* Corresponding author. Fax: +86 10 62771160.
E-mail address: biomater@mail.tsinghua.edu.cn (Q. Feng).

0022-4596/$ - see front matter © 2011 Elsevier Inc. All rights reserved.
doi:10.1016/j.jssc.2011.03.008

are of great importance for the physicochemical properties of the polymer, such as affinity to cations, gelling properties and chain stiffness. Alginate forms gel with divalent cations, such as Ca^{2+}. In the alginate molecules with only G blocks and GM blocks can bind Ca^{2+} in the form of "egg-box", while M blocks act as the solvating moiety [25,26]. Thus, the length of the G blocks is the main structural feature contributing to gel formation [27]. In previous studies, alginate was found to inhibit the crystallization of calcium carbonate by interacting directly with the growing surface of the crystals, although alginate could not alter the standard rhombohedral habit of calcite [28,29]. Butler et al. [2] reported that the direct mixing of calcium and carbonate ions could result in the rosette-like aggregates of calcite in the presence of sodium alginate. Very recently, alginate was used as additives to induce the formation of $CaCO_3$ particles with different shapes and polymorphs [30,31]. For instance, the growth of lens-like vaterite was obtained by slowly released alginate, which was due to the partially oriented aggregation [32]. Despite the importance of alginate in the field of biomineralization, where the polysaccharide provides the template for the intricate hierarchical assembly of calcium carbonate crystals, the research on the precise mechanism of mediating effect of alginate and the interplay between crystallization of calcium carbonate and the biopolymer alginate is so far limited.

In our research, we used a specific strategy, where calcium ion and alginate were slowly and continuously added in the mineralization system. The mineralization process occurred at a relatively low rate. The motivation for this research is to explore how alginate mediates the crystal growth of calcium carbonate. In addition, by studying the possible mineral/biopolymer interactions, the probable mechanism of $CaCO_3$ crystallization within calcium alginate hydrogel is proposed. Generally speaking, the present study provides basic information for the control of calcium carbonate crystals in hydrogel system and suggests a novel pathway for the biomimetic fabrication of functional materials.

2. Experiment section

2.1. Materials

Two different kinds of sodium alginates were used in the experiments, denoted as High G and Low G alginate, respectively. Both of them were purchased from Shanghai Chineway Pharmaceutical Tech. Co. Ltd., Shanghai, China. High G alginate (HG $W_m = 2-3\times10^5$ g/mol, LF 10–60) has 65–75% G blocks and Low G alginate (LG $W_m = 2-3\times10^5$ g/mol, 120 M) has 30–35% G blocks [33]. Higher content of G blocks leads to longer length of G blocks in HG alginate than G blocks in LG alginate. The ratio of G/M blocks is about 7/3 in HG alginate and 3/7 in LG alginate. Fig. 1 reveals the chemical structure of alginate and the arrangement of G and M blocks and repetitive domain of the two alginates for this study. Calcium chloride (AR) and sodium carbonate (AR) were bought from Chemical Agents Co. Ltd., Beijing, China. All chemicals were used without further purification. Deionized water was used throughout the sample preparations.

2.2. Hydrogel preparation and crystallization of $CaCO_3$

For comparison, sodium alginates with different G blocks were used to form the hydrogels and then they were simultaneously setup under the same experimental conditions of calcium carbonate crystallization. 100 ml aqueous sodium alginate solutions (1 w%) were added into 200 ml calcium chloride solutions with 0.02 and 0.1 mol/L concentrations, respectively, via using a disposable syringe. Ca-alginate gel beads with a diameter of approximately 2 mm formed immediately. Then the gel beads were immersed in the calcium chloride solutions overnight. After that the obtained Ca-alginate gel beads (~150 g) were washed with deionized water, dried and put into 200 ml sodium carbonate solutions with 0.02 and 0.1 mol/L concentrations, respectively. The mineralization process lasted for 4 h. The advantage of this procedure is that Ca^{2+} and the alginate macromolecules were gradually released from the Ca-alginate gel with the gel dissociation. When the mineralization process finished, the supernatants were removed carefully, then the calcium carbonate powder precipitated at the bottom of beaker was rinsed, dried and collected. The final $CaCO_3$ powder obtained from High G Ca-alginate gels, which was formed using 0.1 mol/L calcium chloride solutions and 0.1 mol/L sodium carbonate solutions, was named HG01. The $CaCO_3$ powder named HG002 was acquired from High G Ca-alginate gel with 0.02 mol/L calcium chloride solution and 0.02 mol/L sodium carbonate solutions. Calcium carbonate powders LG01 and LG002 were named in the same way. The reactions were carried out at room temperature and the specific procedure is shown in Fig. 2.

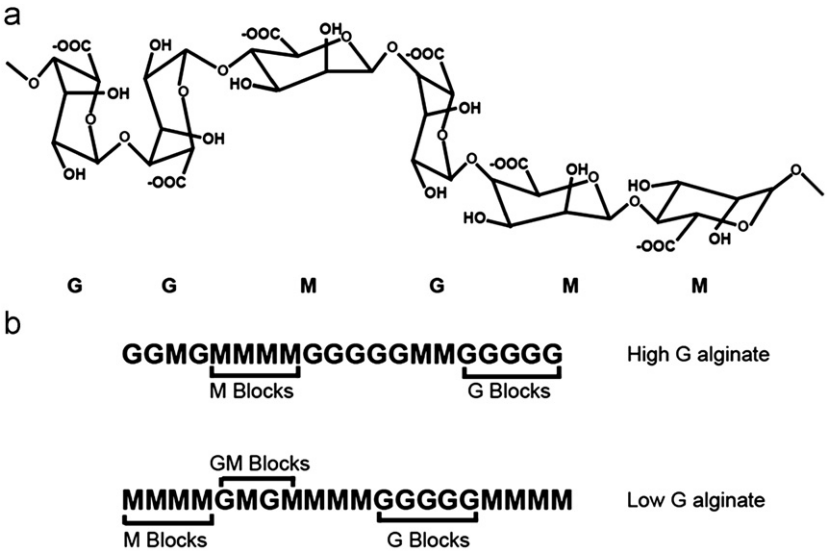

Fig. 1. Chemical structure of alginate (a) and the arrangement of G and M blocks of High G and Low G alginate (b).

2.3. Crystal characterization

When the mineralization process completed, the calcium carbonate named LG01, LG002, HG01 and HG002 were gained. These four kinds of powders were coated with Au prior and then imaged using LEO-1530 (LEO Company) scanning electron microscope (SEM), fitted with a field-emission source operating at an accelerating voltage of 10 kV. Phase analysis was performed by powder XRD using a D8 ADVANCE (BRUKER Company) X-ray diffractometer with Cu $K\alpha$ radiation (40 kV, 40 mA). XRD patterns of calcium carbonate crystals were collected at a 2θ range of 5–80°. Thermogravimetric analysis (TGA) was performed with a TGA Q5000 (TA Instruments) to monitor the weight loss of the samples at a heating rate of 10 °C/min from room temperature to 900 °C under a nitrogen atmosphere. Infrared spectra were collected using a Nicolet 6700 (ThermoFisher SCIENTIFIC) Fourier transform infrared spectrometer using the KBr pellets method with resolution of 4 cm^{-1}. For the time-dependent experiments, the calcium carbonate crystallization reactions were stopped at the designed time. The products were lyophilized to obtain the cotton-like mixtures of alginate and $CaCO_3$, which were directly characterized by FTIR to determine the interplay between mineral and biopolymer.

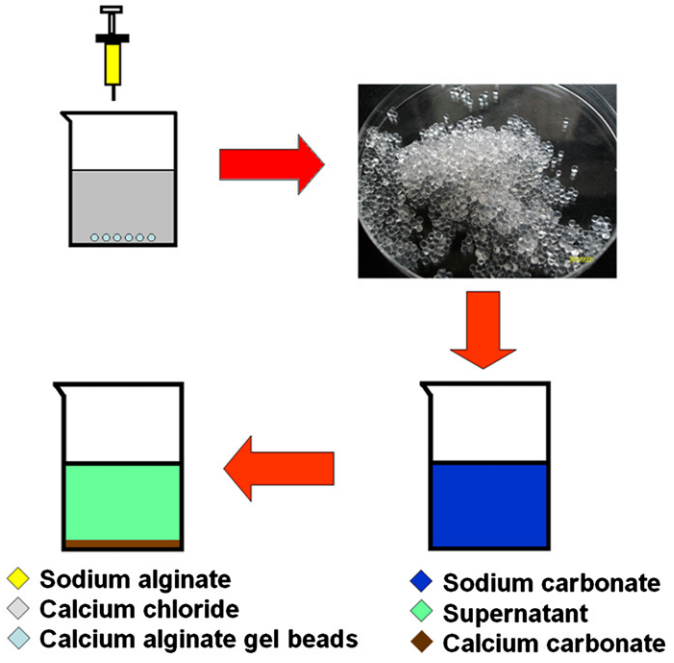

Fig. 2. Schematic diagram of preparing calcium alginate hydrogels and crystallization process of calcium carbonate.

3. Results and discussion

3.1. Calcium carbonate crystal growth with High G and Low G Ca-alginate gels

Four kinds of calcium carbonate samples named HG01, HG002, LG01 and LG002 were used to investigate crystal polymorph by means of powder XRD analysis and FTIR spectral analysis. Fig. 3 depicts the typical XRD patterns of four calcium carbonate crystals and it clearly exhibits that this four obtained $CaCO_3$ crystals have a similar pattern. The diffraction peaks at 2θ of 29.4°, 35.9° and 39.5° correspond to (1 0 4), (1 1 0) and (1 1 3) crystallographic planes of calcite, respectively, while the peak at 43.7° corresponds to (3 0 0) crystallographic plane of vaterite [34]. As indicated by the figure, the displayed diffraction peaks are well in agreement with the previous study. FTIR spectra of calcium carbonate crystals are shown in Fig. 4. The FTIR spectrum of calcite has a particularly interesting characteristic. It has a very intense broad band centering at 1425 cm^{-1} and sharp bands at 876 and 712 cm^{-1}, which can be attributed to ν3 (asymmetric CO stretching) mode, ν2 (CO_3 out-of-plane deformation) mode and ν4 (OCO bending in-plane deformation) mode vibrations [35], respectively. The infrared spectra at 1084 cm^{-1} is attributed to ν1 (symmetric CO stretching) mode of vaterite [36]. Both XRD and FTIR results mentioned above indicate that the synthesized $CaCO_3$ crystals are mainly calcite with a small amount of vaterite crystals.

SEM of calcium carbonate products obtained from the reactions in alginate gels with different length of G blocks and different ion concentrations reveal the different morphology and crystal size of $CaCO_3$ (Fig. 5). In general, there are two kinds of obvious morphologies, one is single calcite crystal and the other is calcite aggregate. The particles of LG002, with morphologies of well-defined rhombohedral single calcite crystals and step-like calcite aggregates, are formed with Low G alginate gel and the CO_3^{2-} concentration of 0.02 mol/L (Fig. 5a). The morphologies of HG002 are similar to that of LG002 (Fig. 5c). The particle size of LG002 and HG002 are about 4.5 and 3.0 μm, respectively. When the ion concentration increased from 0.02 to 0.1 mol/L, the morphologies of calcite crystals changed significantly. The single calcite crystals of LG01 and HG01 transformed from sharp rhombohedral shape to

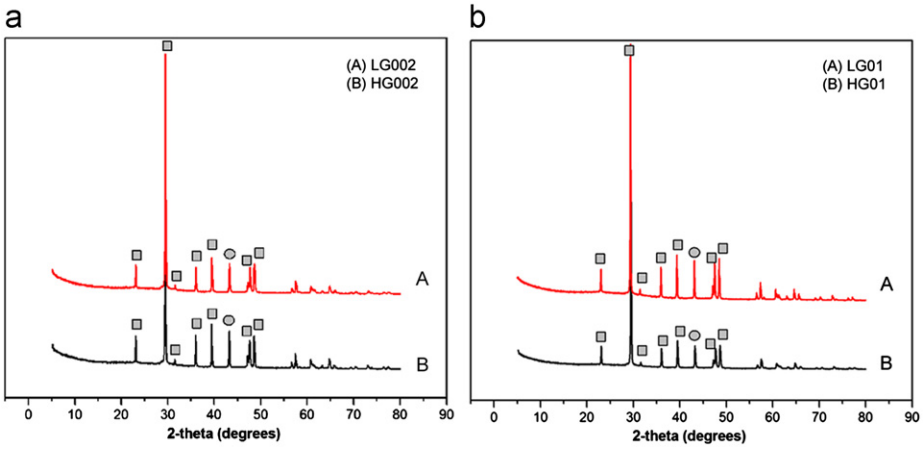

Fig. 3. XRD patterns of $CaCO_3$ precipitated in the present of Low G and High G alginate at different concentrations of carbonate ions. Concentration of carbonate ions: (a) 0.02 mol/L and (b) 0.1 mol/L; Square: calcite, Circle: vaterite.

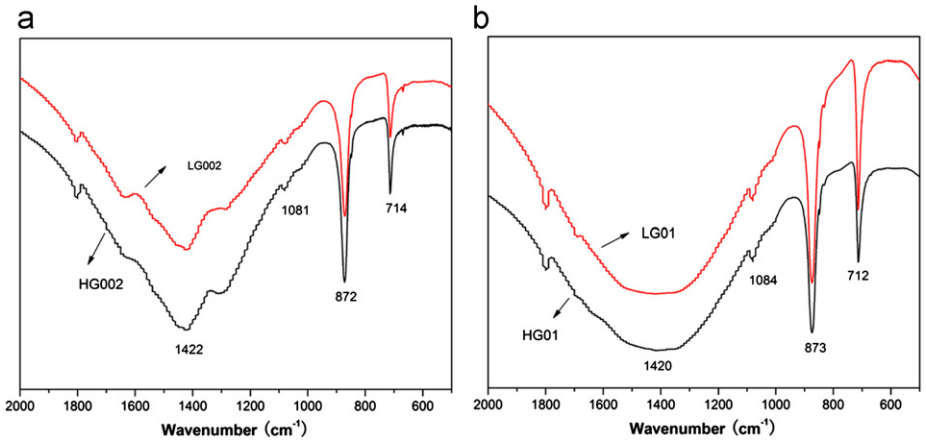

Fig. 4. FTIR spectra of $CaCO_3$ precipitated in the present of Low G and High G alginate at different concentrations of carbonate ions. Concentration of carbonate ions: (a) 0.02 mol/L and (b) 0.1 moI/L.

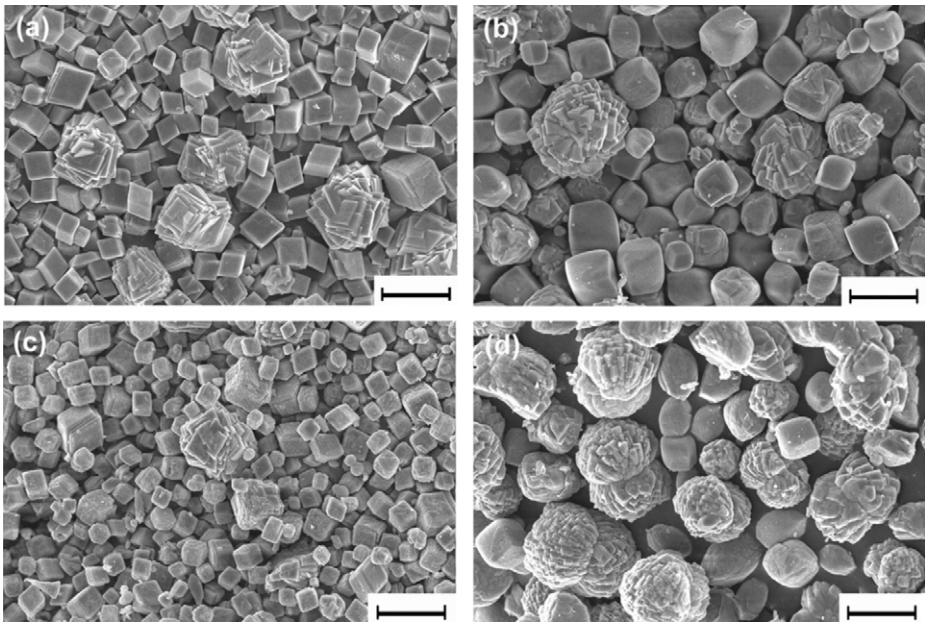

Fig. 5. SEM images of calcium carbonate products obtained from the reactions with different carbonate ion concentrations and mediated by Low G and High G alginate. (a) LG002, (b) LG01, (c) HG002, and (d) HG01; the scale bars in the whole micrographs are 10 μm.

cubic morphology without clear straight edge, and the average crystal sizes are 7.6 and 6.0 μm, respectively (Fig. 5b and d). The calcite aggregates of LG01 with spherical morphology are composed of staircase-like blocks with the exposed (1 0 4) crystalline faces (Fig. 5b), while the aggregates of HG01 show double spherical morphology (Fig. 5d). Interestingly, HG01 displays the same superstructure as the aggregates of LG01. To further investigate the details of morphology, the calcite aggregates of four kinds of particles are magnified, as shown in Fig. 6. Surprisingly, the distinct appearances of crystal surface are detected. The surfaces of crystals mediated by Low G alginate are smooth, regardless of the CO_3^{2-} concentration (i.e. 0.1 or 0.02 mol/L). Comparatively, the surfaces of $CaCO_3$ particles mediated by High G alginate are rough and imperfect.

Alginate was reported previously to exert some influences on the crystallization of $CaCO_3$, but did not alter the standard rhombohedral habit of calcite [29]. However, some literatures do support that the polymorph can be changed in the presence of alginate. Leng et al. [32] believed that alginate exerted a strong stabilizing effect on vaterite, which may originate from the special interaction between alginate and Ca^{2+}. In addition, when sodium alginate was used for the prior treatment of porcine and human heart valves, the crystallization of vaterite on the surfaces of atherosclerotic aorta can be effectively inhibited [37]. Vaterite is usually found when calcium carbonate precipitates at higher levels of supersaturation. In this study, the network structure of macromolecule was existed during the mineralization process [38], in both the High G and the Low G alginate gels. The increase of calcium ion concentration in the macromolecule network produced a high supersaturation of calcium ions at the local sites and then a small amount of vaterite crystals were formed finally.

The method we developed here is targeted for adding the inorganic ions and organic additives, namely Ca^{2+} and alginate molecules to the mineralization system slowly and continuously. The mediating function of alginate was synergistic with the nucleation and growth of $CaCO_3$. The CO_3^{2-} diffusion method used made sure that the CO_3^{2-} concentration within hydrogel increased gradually. CO_3^{2-} was able to capture Ca^{2+} from the gel, which resulted in two cases of calcium carbonate crystal nucleation. One was the selective nucleation of $CaCO_3$ within the Ca-alginate gels;

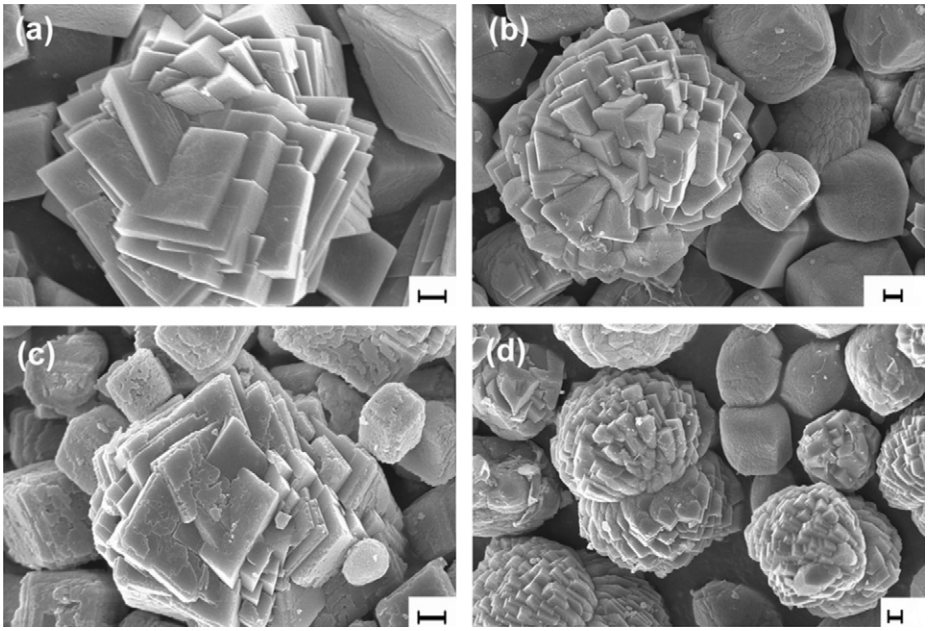

Fig. 6. SEM images of magnified calcite aggregates. (a) LG002, (b) LG01, (c) HG002, and (d) HG01; the scale bars in the whole micrographs are 1 μm.

the other was $CaCO_3$ nucleation in the solution with free alginate molecules. As the Ca^{2+} was captured in the process of gel dissociation, the alginate molecules might exist in two forms, one was Ca-alginate hydrogels and the other was free alginate molecules, till the gels completely dissociated. Therefore, during the whole biomineralization process, $CaCO_3$ crystal growth was mediated by alginate hydrogels and free alginate molecules. The former led to the formation of calcite aggregates and the latter favored the single calcite crystals. From Fig. 5, the crystal size of the single calcite differed in the reactions with different carbonate ion concentrations and mediated by Low G and High G alginates. There might be two factors attributed to the crystal size of calcium carbonate, CO_3^{2-} concentration and the type of alginate molecules. There is no doubt that the higher CO_3^{2-} concentration can provide more ions to promote crystals growth. The effect of the free alginate molecules on the size of $CaCO_3$ will be further discussed later. Previously, Butler et al. [2] reported that the nucleation of calcium carbonate crystals was not inhibited but the induction time was increased in the presence of alginate, leading to the increase in the amount of crystals. Very recently, some researchers have proven that the induction time increased more with High G alginate than with Low G alginate [30]. Considering the smaller size of the calcite crystals with High G alginate, the amount of crystals formed with High G alginate may be much more than that formed in the presence of Low G alginate. On the other hand, alginate is effective in inhibiting calcium carbonate crystallization, which is consistent with previous studies [29,39,40]. Reduced growth of calcium carbonate in the presence of additives is usually accounted for the adsorption of the additives onto active growth sites of the crystal surface and blocking the active growth sites subsequently [29,41]. Because of alginate's high affinity to calcium, it is possible that alginate adsorbed onto active growth sites on the crystal surface, and thus reduced the activity-based calcium carbonate supersaturation, which is probably responsible for the decreased growth rate of $CaCO_3$. It is shown that peptides rich in aspartic and glutamic acid containing carboxylic side groups interacted strongly with calcium carbonate crystal surfaces [42]. In alginate, each monomer contains a carboxylic group, which increases the mineral/biopolymer interaction. The different growth rates for High G and Low G alginate may be accounted for the difference in the length of G blocks, which is an important parameter related to calcium affinity. Thus, the High G alginate with longer G blocks may bind much strongly to the crystal surface, which leads to lower growth rate and stronger growth inhibition of calcium carbonate. It is a probable explanation as why the crystal size controlled by High G alginate is smaller than the one with Low G alginate. Some literature reported that the surface morphological discrepancy is potentially due to the different gelation mechanisms of calcium alginate at different pH [43–45]. We believe that High G alginate can bind to the $CaCO_3$ surface more intensely and interact with the mineral more drastically than Low G alginate, which can lead to the rough and imperfect surface of calcite with High G alginate and the smooth surface with Low G alginate.

3.2. *Interplay between the mineral and the biopolymer in the biomineralization process*

Thermogravimetric analysis (TGA) was employed to determine whether the samples obtained from High G and Low G alginate contain the organic matrix. TGA curves for both HG01 and LG01 are shown in Fig. 7, where the remaining sample weight (%) is plotted as a function of temperature. From the results of TGA, the distinct differences in the two samples are observed. The curve of HG01 shows two weight loss stages. One is probably due to the loss of biopolymer up to about 500 °C. A subsequent loss in mass is observed at approximately 600 °C, which is similar to the case of the pure calcium carbonate sample. The curve of LG01 only shows a loss in mass at 600–700 °C. TGA data for alginate and $CaCO_3$ are reported previously, where the weight loss between 150 and 500 °C is contributed to the decomposition of alginate [46], above 600 °C is due to the decomposition of $CaCO_3$ into CaO and CO_2 [47]. This is consistent with our observations. The researchers had proven that some block copolymers are present in the calcite, and it is believed that there is a strong interaction between functional groups in the polymer and calcium ions in the crystal [48]. Etching experiments on large numbers of calcite crystals obtained from gel system showed that all of the gel-grown crystals incorporated the gel matrix [49]. Further study confirmed that the alginate was involved in the

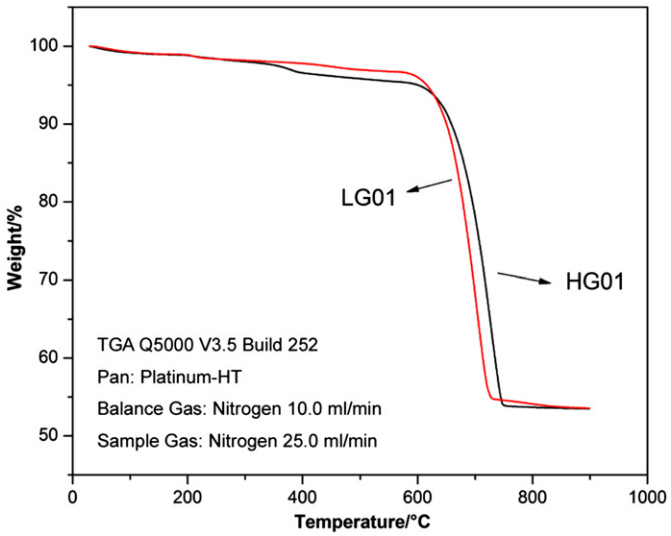

Fig. 7. TGA curves recorded for HG01 and LG01, showing thermal decomposition of the mineralized products.

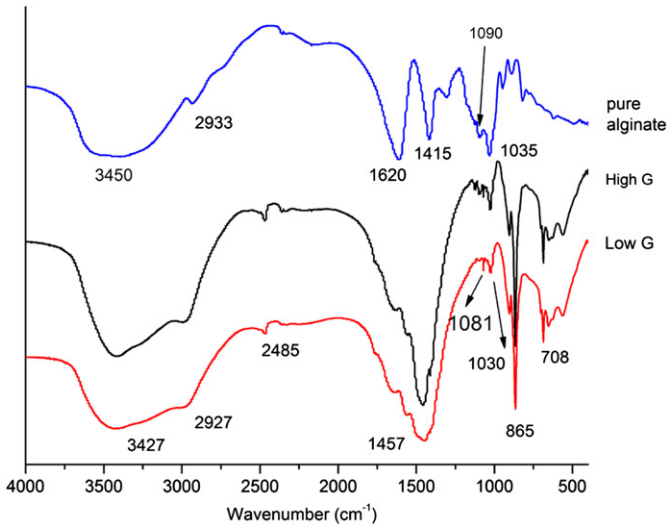

Fig. 8. FTIR spectra of pure alginate and the mixtures obtained at the reaction time of 2 min.

calcium carbonate particles and the particles were $CaCO_3$/alginate hybrids [32]. In the current studies, the alginate is detected in the sample of HG01 rather than LG01, which is probably attributed to the length of G blocks. The High G alginate containing longer G blocks can result in a stronger interplay between the calcium carbonate crystal and the alginate than that of Low G alginate. In addition, the alginate may also exist in LG01, but the amount of alginate is too small to be observed.

During the time-dependent experiments of $CaCO_3$ mineralization, the reactions were stopped at the pre-selected time at 2, 5, 15, 30, 45 and 60 min, and the samples were lyophilized to characterize the mineralization process of $CaCO_3$ by FTIR, This is primarily for determining the interplay between the mineral and biopolymer in the biomineralization process. The variations of infrared absorption peaks and the appearance of new absorption bands are shown in Fig. 8, which describes the FTIR results of pure alginate and the mixtures of crystal and biopolymer obtained after 2-min reaction. As indicated by the curve of the pure alginate, the absorption peaks at 1620 and 1415 cm^{-1} can be assigned to the asymmetric and the symmetric stretching vibration of $-COO^-$ groups, respectively [50,51]. When the reaction time is 2 min, the mineralization of $CaCO_3$ can be confirmed by the appearance of the absorption peaks at 2485, 865 and 708 cm^{-1}, and the peak position shifts to lower wave numbers compared to the standard calcite [35], which indicates that calcite crystallizes at the initial stage and no other polymorph of calcium carbonate is formed.

FTIR spectra of the crystal/biopolymer mixtures acquired from the High G Ca-alginate gels at the reaction times from 5 to 60 min are shown in Fig. 9. The spectra of these samples are similar to each other and only slight differences can be observed in the shape and intensity of the bands. The FTIR spectra, with the bands of asymmetric stretching (1411 cm^{-1}), out-of-plane deformation (874 cm^{-1}) and in-plane deformation (713 cm^{-1}) are attributed to calcite [52]. These typical bands can be observed clearly in these five samples derived from the systems lyophilized at different times. At the reaction time of 5 min, there is no obvious absorption band at around 874 cm^{-1}. From 15 to 60 min, the absorption bands at 873 cm^{-1} become stronger and sharper. Similarly, the band at 706 cm^{-1} also strengthens with the increasing reaction time. These results indicate that the calcite content in the mixture increases with the reaction time extension. The bands at approximately 870, 1030, 1452 and 1620 cm^{-1}, which are clearly visible only for alginate [38], can be detected in these five mixtures. Interestingly,

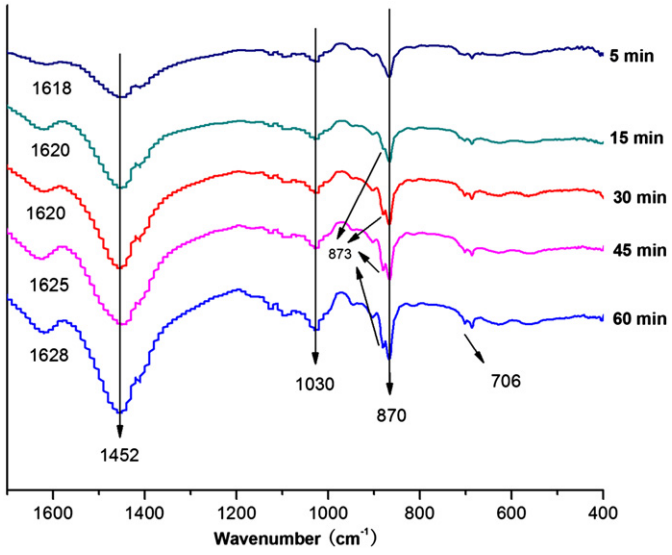

Fig. 9. FTIR spectra of the crystal/bioploymer mixtures acquired from the High G alginate gel at different reaction times.

the absorption band at approximately 1620 cm^{-1}, corresponding to the asymmetrical stretching modes of carboxyl group in alginate (νCOO^-), gradually shifts to higher wavenumber in the samples from 5 to 60 min. These shifts indicate there is chemical interaction between the mineral and the biopolymer, most likely encouraged by the chemical bonding between Ca^{2+} and the negatively charged carboxyl group in alginate [38]. The presence of intermolecular interplay between inorganic minerals and alginate chains in the polymer network can be used to control the crystal size and roughness of the crystal surface.

From the investigations and analyses described previously, the possible mechanism of calcium carbonate crystals with different morphologies formed within the High G and Low G alginate hydrogel is as follow. From the biomineralization's perspective, the biologically controlled process comprises of several coherent steps: extraction and enrichment of calcium and carbonate ions, nucleation, and confined crystallization of $CaCO_3$, arrangement and crystallographic orientation of crystallites [53]. In our study, first of all, G blocks order into "zigzag" structure with cavities of appropriate size for divalent metals. Regions of High G and Low G

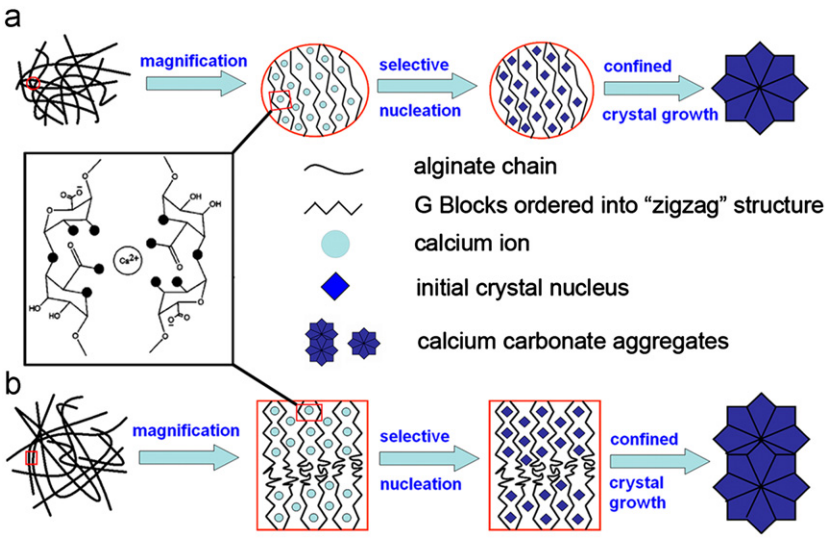

Fig. 10. Schematic illustration of the growth of calcite aggregates with different morphologies obtained from (a) Low G alginate gels and (b) High G alginate gels.

alginate chains rich in G blocks have heightened specificity for Ca^{2+} because of favorable geometric ordering for coordination. This coordinate bond directly leads to the cross-linking of alginate and then calcium alginate hydrogels are formed. Secondly, the slow diffusion of CO_3^{2-} ions onto the gel surface can simulate the extraction and enrichment of carbonate ions. Thirdly, the bound calcium ions in alginate gel can act as the nuclei and then they selectively nucleate together with the diffused carbonate ions to form calcium carbonate crystals. Finally, the *in situ* confined crystallization of $CaCO_3$ takes place within the alginate networks. The confined crystallization leads to the formation of the stair-case-like units with the exposed (1 0 4) crystalline faces and then these units aggregate into a globular shape. In alginate molecules, calcium ions can be bounded by G blocks in the form of "egg-box", where the calcium carbonate nucleated and crystallized [25,26]. Due to the fact that the content of guluronic acid residues is different in High G and Low G alginate, the length of G blocks and the interval blocks (M blocks) differ remarkably between High G and Low G alginate. The High G alginate has shorter intervals in the macromolecule backbones, which makes the two G blocks more compact than that in Low G alginate. This explains to some extent why double spherical calcite aggregates are formed with High G alginate gels, while single spherical calcite aggregates are obtained from Low G alginate gels. Thus, the calcium carbonate mineralization within the network of calcium alginate hydrogel is schematically illustrated in Fig. 10. This summarizes the two steps of $CaCO_3$ crystal formation: selective nucleation and confined crystallization of calcium carbonate.

4. Conclusions

In this paper, we documented a specific method for combining inorganic ions and organic additives slowly and continuously for a better mimicking of the biomineralization process in organisms. SEM and XRD confirmed the effect of alginate on the crystallization of $CaCO_3$. Calcite, with two main morphologies of the single calcite crystals and the spherical calcite aggregates, was the predominant phase and a small amount of vaterite was coexisted. The crystal size, morphology and crystal surface roughness were controlled by the length of G blocks in alginate. FTIR and TGA determined the interplay between the mineral and biopolymer in the mineralization process. There were chemical interactions between the alginate and the mineral phase, which might be assigned to the interplay between calcium ions in the mineral and carboxyl groups in alginate. A potential mechanism of $CaCO_3$ crystallization within calcium alginate hydrogel was proposed. The selective nucleation and the subsequent confined crystallization of $CaCO_3$ within the decomposed calcium alginate hydrogel with High G and Low G blocks led to form the double spherical calcite aggregates and single spherical calcite aggregates, respectively. Although detailed crystallographic data of $CaCO_3$ were not available from the present study, the results demonstrated important aspects of alginate-controlled crystallization, which contributed to the understanding of mineralization process in hydrogel systems and suggested a novel pathway for the biomimetic fabrication of functional materials.

Acknowledgments

We are grateful for the financial support from the 973 project (2007CB815604), National Natural Science Foundation of China (51072090) and NSFC-ANR (51061130554).

References

[1] S. Mann, Biomineralization: Principles and Concepts in Bioinorganic Materials Chemistry, Second ed., Oxford University Press, New York, 2001.
[2] M.F. Butler, N. Glaser, A.C. Weaver, M. Kirkland, M. Heppenstall-Butler., Cryst. Growth Des. 6 (2006) 781–794.
[3] H. Cölfen, Curr. Opin. Colloid In. 8 (2003) 23–31.
[4] S. Mann, C.C. Perry., Adv. Inorg. Chem. Radiat 36 (1991) 137–200.
[5] Z.F. Mao, J.H. Huang., J. Solid State Chem. 180 (2007) 453–460.
[6] L.H. He, R. Xue, R. Song, J. Solid State Chem. 182 (2009) 1082–1087.
[7] N. Sommerdijk, G. de With, Chem. Rev. 108 (2008) 4499–4550.
[8] F.C. Meldrum, H. Cölfen, Chem. Rev. 108 (2008) 4332–4432.
[9] J.G. Yu, X.F. Zhao, B. Cheng, Q.J. Zhang, J. Solid State Chem. 178 (2005) 861–867.
[10] J.G. Yu, M. Lei, B. Cheng, X.J. Zhao, J. Solid State Chem. 177 (2004) 681–689.
[11] T.P. Wang, M. Antonietti, H. Cölfen, Chem.-Eur. J 12 (2006) 5722–5730.
[12] T.X. Wang, H. Cölfen, M. Antonietti, J. Am. Chem. Soc. 127 (2005) 3246–3247.
[13] J.J.J.M. Donners, R.J.M. Nolte, N.A.J.M. Sommerdijk, J. Am. Chem. Soc. 124 (2002) 9700–9701.
[14] C. Cheng, Z.Z. Shao, F. Vollrath, Adv. Funct. Mater. 18 (2008) 2172–2179.
[15] S. Raz, S. Weiner, L. Addadi, Adv. Mater. 12 (2000) 38–42.
[16] G. Falini, S. Albeck, S. Weiner, L. Addadi, Science 27 (1996) 67–69.
[17] A.M. Belcher, X.H. Wu, R.J. Christensen, P.K. Hansma, G.D. Stucky, D.E. Morse, Nature 381 (1996) 56–58.
[18] J.L. Arias, M.S. Fernandez, Chem. Rev. 108 (2008) 4475–4482.
[19] G. Falini, S. Fermani, A. Ripamonti, J. Inorg. Biochem. 91 (2002) 475–480.
[20] Y. Yamamoto, T. Nishimura, T. Saito, T. Kato, Polym. J. 42 (2010) 583–586.
[21] A. Sugawara, A. Oichi, H. Suzuki, Y. Shigesato, T. kogure, T. Kato, J. Polym. Sci. Part A: Polym. Chem. 44 (2006) 5153–5160.

[22] T. Nishimura, T. Ito, Y. Yamamoto, M. Yoshio, T. Kato, Angew. Chem. Int. Ed. 120 (2008) 2842–2845.
[23] G. Falini, S. Fermani, Tissue Eng. 10 (2004) 1–6.
[24] A. Haug, B. Larsen, O. Smidsrod, Acta Chem. Scand. 20 (1966) 183–200.
[25] Y.P. Fang, S. Al-Assaf, G.O. Phillips, K. Nishinari, T. Funami, P.A. Williams, L.B. Li, J. Phys. Chem. B 111 (2007) 2456–2462.
[26] I. Donati, S. Holtan, Y.A. Morch, M. Borgogna, M. Dentini, G. Skjak-Braek, Biomacromolecules 6 (2005) 1031–1040.
[27] G. Skjakbraek, O. Smidsrod, B. Larsen, Int. J. Biol. Macromol. 8 (1986) 330–336.
[28] D.L. Verraest, J.A. Peters, H. v anBekkum, G.M. vanRosmalen, J. Am. Oil Chem. Soc. 73 (1996) 55–62.
[29] F. Manoli, E. Dalas, J. Mater. Sci.: Mater. Med 13 (2002) 155–158.
[30] M.Ø. Olderøy, M.L. Xie, B.L. Strand, E.M. Flaten, P. Sikorski, J.P. Andreassen, Cryst. Growth Des. 9 (2009) 5176–5183.
[31] M. Diaz-Dosque, P. Aranda, M. Darder, J. Retuert, M. Yazdani-Pedram, J.L. Arias, E. Ruiz-Hitzky, J. Cryst. Growth. 310 (2008) 5331–5340.
[32] B.X. Leng, F.G. Jiang, K.B. Lu, W.H. Ming, Z.Z. Shao, Crystengcomm 12 (2010) 730–736.
[33] R.W. Tan, X.F. Niu, S.L. Gan, Q.L. Feng, J. Mater. Sci.: Mater. Med 20 (2009) 1245–1253.
[34] Y.H. Shen, A.J. Xie, Z.X. Chen, W.H. Xu, H. Yao, S.K. Li, L.C. Huang, Z.F. Wu, X.Y. Kong, Mater. Sci. Eng. A—Struct 443 (2007) 95–100.
[35] F.A. Andersen, L. Brecevic, Acta Chem. Scand. 45 (1991) 1018–1024.
[36] J.R. Clarkson, T.J. Price, C.J. Adams, J. Chem. Soc. Faraday Trans. 88 (1992) 243–249.
[37] J. Kanakis, P. Malkaj, J. Petroheilos, E. Dalas, J. Cryst. Growth. 223 (2001) 557–564.
[38] M.L. Xie, M.Ø. Olderøy, J.P. Andreassen, S.M. Selbach, B.L. Strand, P. Sikorski, Acta Biomater. 6 (2010) 3665–3675.
[39] J.M. Didymus, P. Oliver, S. Mann, A.L. Devries, P.V. Hauschka, P. Westbroek, J. Chem. Soc. Faraday Trans. 89 (1993) 2891–2900.
[40] L. Yang, X.Y. Zhang, Z.J. Liao, Y.M. Guo, Z.G. Hu, Y. Cao, J. Inorg. Biochem. 97 (2003) 377–383.
[41] B. Njegic-Dzakula, L. Brecevic, G. Falini, D. Kralj, Cryst. Growth Des. 9 (2009) 2425–2434.
[42] R.A. Metzler, I.W. Kim, K. Delak, J.S. Evans, D. Zhou, E. Beniash, F. Wilt, M. Abrecht, J.W. Chiou, J.H. Guo, S.N. Coppersmith, P. Gilbert, Langmuir 24 (2008) 2680–2687.
[43] P. Matricardi, M. Pontoriero, T. Coviello, M.A. Casadei, F. Alhaique, Biomacromolecules 9 (2008) 2014–2020.
[44] I. Donati, J.C. Benegas, A. Cesaro, S. Paoletti, Biomacromolecules 7 (2006) 1587–1596.
[45] H.J. Kong, C.J. Kim, N. Huebsch, D. Weitz, D.J. Mooney, J. Am. Chem. Soc. 129 (2007) 4518–4519.
[46] A. Pourjavadi, M. Samadi, H. Ghasemzadeh, Macromol. Symposia. 274 (2008) 177–183.
[47] M. Faatz, F. Grohn, G. Wegner, Adv. Mater. 16 (2004) 996–1000.
[48] R. Dimova, R. Lipowsky, Y. Mastai, M. Antonietti, Langmuir 19 (2003) 6097–6103.
[49] H.Y. Li, L.A. Estroff, Crystengcomm 9 (2007) 1153–1155.
[50] D. Leal, B. Matsuhiro, M. Rossi, F. Caruso, Carbohyd. Res. 343 (2008) 308–316.
[51] S.K. Tam, J. Dusseault, S. Polizu, M. Menard, J.P. Halle, L. Yahia, Biomaterials 26 (2005) 6950–6961.
[52] A.G. Xyla, P.G. Koutsoukos, J. Chem. Soc. Faraday Trans. 1 (1989) 3165–3172.
[53] X.P. Li, Q. Shen, Y.L. Su, F. Tian, Y. Zhao, D.J. Wang, Cryst. Growth Des. 9 (2009) 3470–3476.